Mesoporous Metals Hot Paper

Deutsche Ausgabe: DOI: 10.1002/ange.201505232
Internationale Ausgabe: DOI: 10.1002/anie.201505232

Polymeric Micelle Assembly for the Smart Synthesis of Mesoporous Platinum Nanospheres with Tunable Pore Sizes

Yunqi Li, Bishnu Prasad Bastakoti, Victor Malgras, Cuiling Li, Jing Tang, Jung Ho Kim, and Yusuke Yamauchi**

Abstract: *A facile method for the fabrication of well-dispersed mesoporous Pt nanospheres involves the use of a polymeric micelle assembly. A core–shell–corona type triblock copolymer [poly(styrene-b-2-vinylpyridine-b-ethylene oxide), PS-b-P2VP-b-PEO] is employed as the pore-directing agent. Negatively charged $PtCl_4^{2-}$ ions preferably interact with the protonated $P2VP^+$ blocks while the free PEO chains prevent the aggregation of the Pt nanospheres. The size of the mesopores can be finely tuned by varying the length of the PS chain. Furthermore, it is demonstrated that the metallic mesoporous nanospheres thus obtained are promising candidates for applications in electrochemistry.*

Recently, materials with ultralarge mesopores have become a subject of extensive research because they can lead to a fast and efficient transport of reactants or effectively adsorb large molecules.[1] Zhao et al. demonstrated that mesoporous Au/silica materials with ultralarge ordered mesopores exhibited an excellent catalytic activity owing to their high surface area and efficient mass transport.[2] Mesoporous carbon spheres with similar pore sizes were fabricated by using a high-molecular-weight diblock copolymer, poly(styrene-*b*-ethylene oxide) (PS-*b*-PEO), as a template and exhibited high electrochemical activity owing to the less restricted diffusion of guest species.[3] Mesoporous silica nanoparticles with pore sizes larger than big biomacromolecules (e.g., proteins, DNA) were shown to be an excellent candidate for drug-delivery systems.[4] Thus far, most of the studies on materials with ultralarge mesopores were limited to traditional compositions (e.g., silica, carbon, and metal oxides),[5] whereas the synthesis of metallic materials with such structural features remains a challenge.

Soft templating is a very popular approach to prepare mesoporous metals. Low-molecular-weight amphiphilic molecules (e.g., Brij 58, P123, and F127) have mostly been utilized as pore-directing agents, where the hydrophilic PEO units accommodate the metal sources.[6] Electrochemical or chemical reduction of the metal precursors is generally involved in the preparation of mesoporous metal films or powders.[7] However, the use of low-molecular-weight surfactants can only produce small mesopores (smaller than 10 nm), which ultimately limits the mobility of guest molecules and further devalues the electrocatalytic performance. Therefore, high-molecular-weight block copolymers, such as PS-*b*-PEO, have previously been used to overcome this issue. Our group reported the formation of cage-type mesoporous Pt particles with a pore size of 15 nm by the electrochemical deposition of lyotropic liquid crystals (LLCs) containing PS-*b*-PEO diblock copolymers.[8] The same block copolymer can also be used to prepare mesoporous Pd nanoparticles with a rather broad particle size distribution.[9] Block-copolymer-based syntheses thus have several advantages in the preparation of particles with large mesopores. However, monodisperse mesoporous metal particles with uniform sizes have never been reported, probably owing to the lack of controlled reactive domains in the polymer backbone as well as the unavoidable aggregation of micelles during the synthesis.

To overcome the aforementioned issues, this work focuses on a core–shell–corona type poly(styrene-*b*-2-vinylpyridine-*b*-ethylene oxide) (PS-*b*-P2VP-*b*-PEO) triblock copolymer to guide the formation of mesopores with a tunable size leading to Pt nanospheres with promising properties as electrocatalysts (Figure 1). Three different triblock copolymers, PS_{192}-*b*-$P2VP_{143}$-*b*-PEO_{613}, PS_{31}-*b*-$P2VP_{12}$-*b*-PEO_{409}, and PS_{432}-*b*-$P2VP_{247}$-*b*-PEO_{1862} (abbreviated as PS_{192}, PS_{31}, and PS_{432}), were used in this study. The pH-sensitive P2VP block is protonated in acidic media and can serve as a much more efficient metal-binding block than PEO. The outer, free PEO block acts as a micelle stabilizer through steric repulsion while the hydrophobic PS block enables the formation of a frozen core in water and dictates the diameter of the mesopore. The beauty of this method is that the mesoporous structure is well-maintained after removing the template by calcination, and the pore size can be easily tuned by adjusting the molecular weight of the PS block. Even the largest pore size of approximately 35 nm was realized without pore-expanding agents. The new mesoporous Pt nanospheres with large pore sizes exhibit an excellent electrocatalytic performance.

[*] Y. Li, Dr. B. P. Bastakoti, Dr. V. Malgras, Dr. C. Li, J. Tang, Prof. Y. Yamauchi
World Premier International (WPI) Research Center for Materials Nanoarchitectonics (MANA)
National Institute for Materials Science (NIMS)
1-1 Namiki, Tsukuba, Ibaraki 305-0044 (Japan)
E-mail: yamauchi.yusuke@nims.go.jp
bishnubastakoti@hotmail.com
Homepage: http://www.yamauchi-labo.com
Y. Li, J. Tang, Prof. Y. Yamauchi
Faculty of Science and Engineering, Waseda University
3-4-1 Okubo, Shinjuku, Tokyo 169-8555 (Japan)
Prof. J. H. Kim
Institute for Superconducting and Electronic Materials
Australian Institute for Innovative Materials
University of Wollongong
Fairy Meadow, North Wollongong, NSW 2500 (Australia)

Supporting information for this article is available on the WWW under http://dx.doi.org/10.1002/anie.201505232.

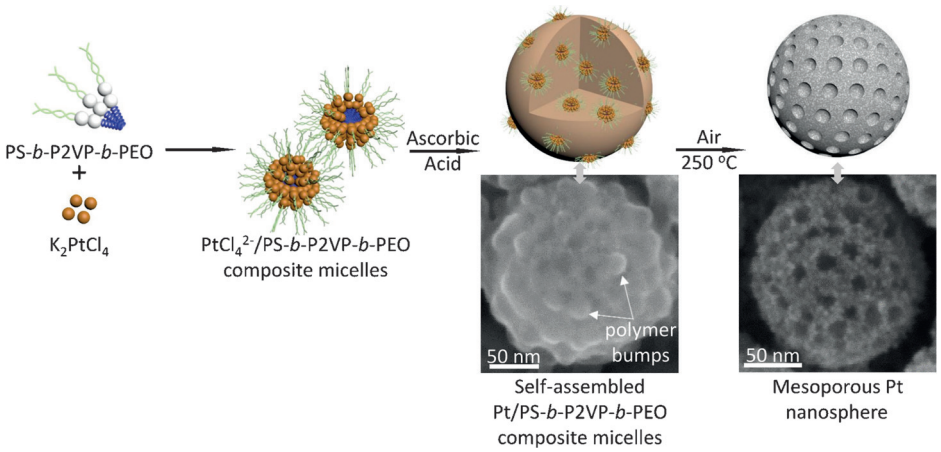

Figure 1. Synthesis of mesoporous Pt nanospheres with tunable pore sizes by making use of a polymeric micelle assembly.

a fringe spacing of 0.23 nm and a dihedral angle of approximately 70°, which can be assigned to the (111) plane of a *fcc* crystal.[11] The multiple spots visible on the selected-area electron diffraction (SAED) pattern highlight the polycrystalline nature of the structure (Figure S4c). The wide-angle XRD profile (Figure S1e) confirms the *fcc* crystal structure as the (111), (200), (220), and (311) diffraction peaks could be assigned.

To understand the role of the PS-*b*-P2VP-*b*-PEO copolymer, nonporous Pt nanospheres with

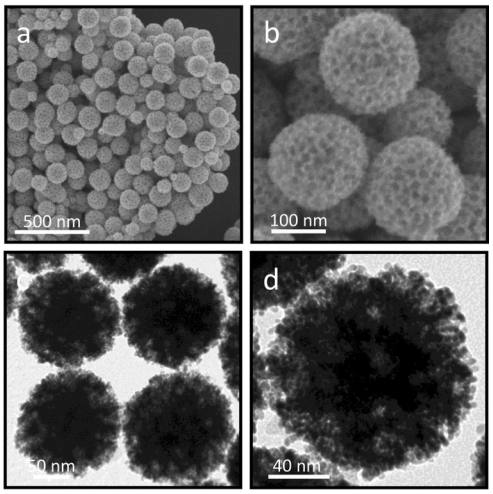

Figure 2. a, b) SEM and c, d) TEM images of mesoporous Pt nanospheres prepared from PS_{192}.

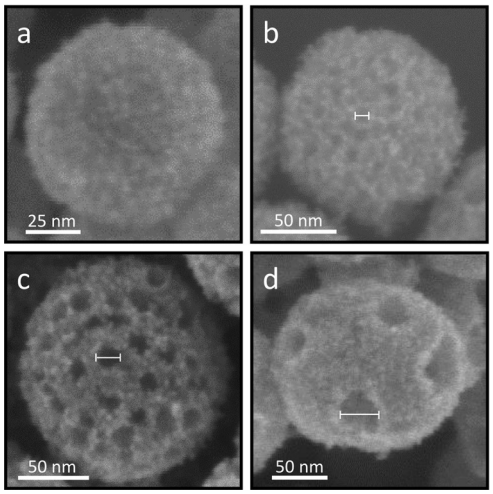

Figure 3. SEM images of mesoporous Pt nanospheres with different pore sizes prepared from different triblock copolymers. a) Without a triblock copolymer, b) with PS_{31}, c) with PS_{192}, and d) with PS_{432}. The mesopores are indicated with straight lines.

The average diameter of the obtained mesoporous Pt nanospheres was determined to be approximately 150 nm by scanning electron microscopy (SEM) and transmission electron microscopy (TEM), and uniformly large mesopores (ca. 14 nm) were distributed over the entire surface of the Pt nanospheres (Figure 2). The low-angle X-ray diffraction (XRD) profile (Supporting Information, Figure S1d) shows a broad peak at 0.38°, which corresponds to a pore-to-pore distance of approximately 23 nm and highlights the uniform mesoporous structure. The obtained N_2 adsorption–desorption isotherm can be categorized as a type IV isotherm with a hysteresis loop at a relative pressure ranging from 0.4 to 0.9 (Figure S2). The surface area was measured to be 30.0 $m^2 g^{-1}$. The Barrett–Joyner–Halenda (BJH) pore-size distribution curve shows that two types of pores coexist, namely mesopores and micropores with a random size distribution from 1 to 4 nm, in addition to a dominating pore size of 14 nm. The micropores originate from the nanovoids (i.e., micropores) between adjacent Pt nanoparticles.[10] High-resolution TEM images (Figure S4) focusing on the edge of a particle reveal a rough surface were synthesized in an aqueous K_2PtCl_4 solution without triblock copolymers under otherwise identical conditions (Figure 3a). It could thus be shown that PS-*b*-P2VP-*b*-PEO acts as a pore-directing agent during the preparation process. Mesoporous Pt nanospheres with different pore sizes, approximately 8, 14, and 35 nm, were synthesized by employing block copolymers with different numbers of PS units (31, 192, and 432, respectively; Figure 3 and Figure S3). The formation of a dense PS core stained by 0.1 wt% phosphotungstic acid was confirmed by TEM (Figure 4a and Figure S5).[12] The sizes of the PS core are approximately 7, 14, and 38 nm, respectively, for the polymers PS_{31}, PS_{192}, and PES_{432}, which are similar to the diameters of the resultant mesopores. The method reported in this work provides an efficient means for controlling the pore size by changing the molecular weight of the PS blocks instead of using pore-expanding agents (e.g., 1,3,5-trimethylbenzene (TMB), 1,3,5-triisopropylbenzene (TIPB), or homopolystyrene (PS_n)).[13]

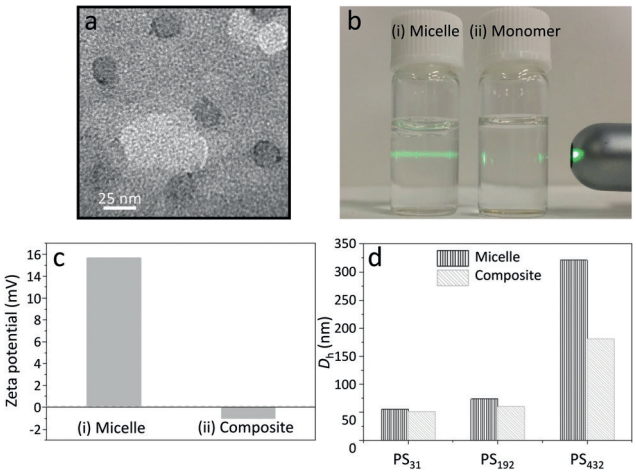

Figure 4. a) TEM image of PS_{192} micelles in which only the PS core was stained with 0.1 wt% phosphotungstic acid. b) Photograph demonstrating the Tyndall effect: The incident light beam is scattered in the presence of micelles. c) Zeta potentials of PS_{192} micelles and $PtCl_4^{2-}/PS_{192}$ composite micelles. d) The shrinking of $PtCl_4^{2-}$/PS-*b*-P2VP-*b*-PEO composite micelles can be deduced from a decrease in the D_h value.

The Tyndall effect was used to determine whether the block copolymers have formed a stable micelle solution (Figure 4b). Dynamic light scattering measurements were performed to determine the hydrodynamic diameter (D_h) of the PS_{192}-*b*-$P2VP_{143}$-*b*-PEO_{613} micelles to be approximately 73.6 nm at pH 3. A zeta potential of + 13.66 mV implies that the protonated $P2VP^+$ blocks tend to interact with negatively charged entities. The $PtCl_4^{2-}$ species serve as counterions for the protonated $P2VP^+$ blocks and can strongly bond with them. After the addition of $PtCl_4^{2-}$, the D_h value and the zeta potential of the composite micelles decreased to approximately 60.1 nm and −1.02 mV, respectively (Figure 4c, d). As a result of the interactions with these anions, the electrostatic repulsion forces between adjacent P2VP blocks become weaker, and therefore, a significant micelle conformational change from swelling to shrinking is observed.[14] Micelles with longer P2VP blocks exhibited a higher degree of shrinkage (Figure 4d). PS_{432}-*b*-$P2VP_{247}$-*b*-PEO_{1862} possessed about 247 units of the protonated $P2VP^+$ blocks at pH 3, and the D_h value was reduced from approximately 321.2 nm to 181.3 nm after complete reaction with $PtCl_4^{2-}$. In contrast, the D_h value changed only from approximately 55.8 nm to 51.5 nm in the case of PS_{31}-*b*-$P2VP_{12}$-*b*-PEO_{40}, which is due to the comparatively small contribution of the short $P2VP^+$ blocks (only 12 units). Several groups have also reported that anionic species selectively interact with protonated $P2VP^+$ blocks at pH < 5.[15] Nakashima et al. demonstrated that negatively charged silica species could strongly bond with ionizable P2VP block copolymers at pH 4, which led to the formation of hollow silica nanospheres.[16] When the surface charge is almost zero, the $PtCl_4^{2-}$/PS-*b*-P2VP-*b*-PEO composite micelles show long-term stability, indicating that the PEO blocks do not lose their hydrophilicity and can maintain the stability of the system in aqueous solution. The PS_{432}-*b*-$P2VP_{247}$-*b*-PEO_{1862} copolymer, which has a long PEO chain, tends to form large pore-to-pore distances (i.e., lower mesopore density; Figure 3d), because very strong steric repulsion forces affect micelle assembly during the Pt deposition.

A mechanism for the formation of mesoporous Pt nanospheres is proposed in Figure 1. An aqueous micelle solution of the triblock copolymer PS-*b*-P2VP-*b*-PEO is first prepared by a dialysis method.[16] Protonated $P2VP^+$ shells are the only binding sites for anionic $PtCl_4^{2-}$ at an early stage of the reaction. The addition of an ascorbic acid solution induces both the Pt deposition and the micelle assembly. The surface of the particles becomes decorated with spherical bumps, which are thought to be spherical block-copolymer micelles (Figure S6). Finally, the as-prepared samples are heated up to 250 °C in air to remove the template.

Calcination is a convenient method to remove block copolymer templates from mesoporous oxide materials. However, such strategies hardly preserve the original morphology of noble-metal nanomaterials. Extractions with organic solvents (e.g., ethanol, THF, or toluene) are commonly employed to remove the template from the mesoporous metals; however, large amounts of volatile and poisonous organic solvents must thus be utilized, and washing periods of considerable length are required.[6–9] We chose to adopt a heat treatment for the removal of the polymer template because large mesoporous noble-metal particles usually exhibit good thermal stability.[9,17] Thermogravimetric measurements (Figure S7) confirmed the successful removal of the triblock copolymer at 250 °C in air. Further increasing the calcination temperature facilitated template removal, but the mesoporous structure tended to collapse above 450 °C owing to the rapid growth of Pt nanoparticles (Figure S1a–c). By analyzing the (111) diffraction peaks of various samples after calcination at 250, 350, and 450 °C with the Scherrer equation, the average sizes of the Pt nanoparticles were calculated to be 6.5, 6.5, and 19.7 nm, respectively, whereas the average crystalline size before calcination was 5.6 nm (Figure S1e). The mesoporous Pt nanospheres obtained after calcination at 250 °C consist of interconnected Pt nanoparticles as determined by TEM (Figure S4b), which is also supported by the presence of a broad peak at approximately 2° on the corresponding low-angle XRD profile (Figure S1d).[18] When the sample was calcined at 450 °C, however, the Pt atoms rearranged significantly,[19] and the fast aggregation of Pt nanoparticles was observed, highlighting the importance of optimizing the thermal treatment to synthesize particles with the desired size and surface morphology.

This new method enables the synthesis of mesoporous structures with a high surface area and interior regions that are easily accessible and can thus take part in electrochemical reactions. Using cyclic voltammetry (CV), the electrochemical surface area (ECSA) was calculated from the charge generated during hydrogen desorption in the potential range of −0.2 to 0.2 V in 0.5 M H_2SO_4 solution (Figure S8).[20] Three samples were investigated: mesoporous Pt nanospheres (pore size: 14 nm), nonporous Pt nanospheres, and commercial Pt black (abbreviated as meso Pt NSs, Pt NSs, and Pt black, respectively). The meso Pt NSs have a larger specific ECSA

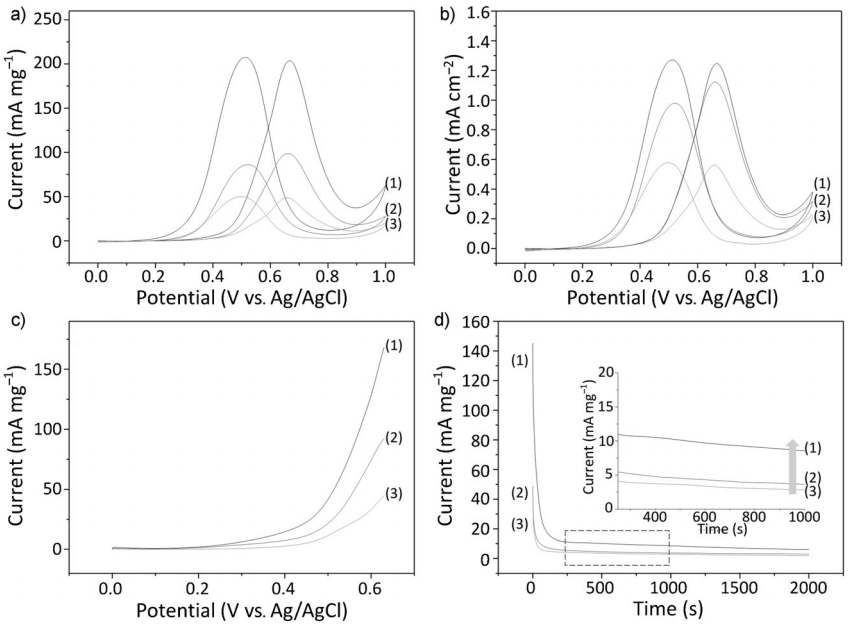

Figure 5. The methanol oxidation reaction catalyzed by 1) mesoporous Pt nanospheres with a pore size of 14 nm, 2) nonporous Pt nanospheres, and 3) commercial Pt black. a, b) Cyclic voltammograms, c) linear sweep voltammograms, and d) chronoamperometric curves at 0.6 V (the inset corresponds to the area indicated by the dashed rectangle) were recorded in an aqueous solution containing 0.5 M H_2SO_4 and 0.5 M methanol. The currents were normalized by the Pt mass, except for the curves shown in panel (b), which were normalized by the ECSA values obtained from the CV curves recorded in 0.5 M H_2SO_4 solution.

(16.34 $m^2 g^{-1}$) than the Pt NSs (8.8 $m^2 g^{-1}$) and Pt black (8.67 $m^2 g^{-1}$), which is due to the presence of a multitude of accessible active sites, especially deep inside the nanospheres. The Pt NSs aggregated significantly (Figure S9a), and Pt black[18] is composed of randomly agglomerated nanoparticles, which usually impedes the access to active sites. Furthermore, the structural stability was tested by cycling treatment in a potential range between −0.2 and 1.5 V. Meso Pt NSs exhibit a high structural stability with a small decrease in ECSA compared to commercial Pt black (Figure S10). In an investigation on their activity in the methanol oxidation reaction (MOR; Figure 5a), two typical anodic peaks could be observed during the forward and backward sweeps,[21] and the meso Pt NSs exhibited the best catalytic performance. The mass-specific current densities of the forward sweep are 203.6, 98.7, and 48.7 mA mg^{-1} for the meso Pt NSs, Pt NSs, and Pt black, respectively. Even when the activity is normalized by the ECSA, the specific current density of the meso Pt NSs (1.24 mA cm^{-2}) is still higher than others (Figure 5b). The superior catalytic activity can be ascribed to their highly crystallized mesoporous structure and easily accessible active sites. Furthermore, the remarkable negative shift of the peak potential and the onset potential determined by linear sweep voltammetry (Figure 5c) indicate an enhanced methanol oxidation for the meso Pt NSs compared to the other two samples. Chronoamperometric measurements performed at 0.6 V (Figure 5d) revealed that the meso Pt NSs show a good activity retention over a period of 2000 s, as the uniform mesoporous structure enhances the accessibility of methanol to catalytically active sites.

In conclusion, we have developed a new and facile method for the synthesis of mesoporous Pt nanospheres with tunable pore sizes. The core–shell–corona type PS-*b*-P2VP-*b*-PEO triblock copolymer plays a key role to direct the formation of mesopores, and each block serves a particular function: The dense hydrophobic PS cores determine the size of the mesopores, the protonated $P2VP^+$ blocks are the binding sites for anionic $PtCl_4^{2-}$, and the hydrophilic PEO coronas are essential for micelle stability and prevent nanosphere aggregation. The mesoporous Pt nanospheres thus obtained were shown to be highly active electrocatalysts for methanol oxidation compared with nonporous nanospheres or commercial Pt black.

Acknowledgements

This research was partially supported by a Grant-in-Aid for Young Scientists A (26708028) of the Japan Society for the Promotion of Science (JSPS), the Japanese-Taiwanese Cooperative Program of the Japan Science and Technology Agency (JST), and The Canon Foundation.

Keywords: block copolymers · mesoporous materials · mesoporous metals · micelles · platinum

How to cite: *Angew. Chem. Int. Ed.* **2015**, *54*, 11073–11077
Angew. Chem. **2015**, *127*, 11225–11229

[1] a) F. Tang, L. Li, D. Chen, *Adv. Mater.* **2012**, *24*, 1504–1534; b) Y. Deng, J. Wei, Z. Sun, D. Zhao, *Chem. Soc. Rev.* **2013**, *42*, 4054–4070; c) J. C. Ndamanisha, L. Guo, *Anal. Chim. Acta* **2012**, *747*, 19–28; d) J. Zhang, C. M. Li, *Chem. Soc. Rev.* **2012**, *41*, 7016–7031.

[2] J. Wei, Q. Yue, Z. Sun, Y. Deng, D. Zhao, *Angew. Chem. Int. Ed.* **2012**, *51*, 6149–6153; *Angew. Chem.* **2012**, *124*, 6253–6257.

[3] J. Tang, J. Liu, C. Li, Y. Li, M. O. Tade, S. Dai, Y. Yamauchi, *Angew. Chem. Int. Ed.* **2015**, *54*, 588–593; *Angew. Chem.* **2015**, *127*, 598–603.

[4] a) I. I. Slowing, B. G. Trewyn, V. S.-Y. Lin, *J. Am. Chem. Soc.* **2007**, *129*, 8845–8849; b) M. Wu, Q. Meng, Y. Chen, Y. Du, L. Zhang, Y. Li, L. Zhang, J. Shi, *Adv. Mater.* **2015**, *27*, 215–222; c) Y. Yang, Y. Niu, J. Zhang, A. K. Meka, H. Zhang, C. Xu, C. X. C. Lin, M. Yu, C. Yu, *Small* **2015**, *11*, 2743–2749.

[5] a) D. Niu, Z. Liu, Y. Li, X. Luo, J. Zhang, J. Gong, J. Shi, *Adv. Mater.* **2014**, *26*, 4947–4953; b) M. Wang, Z. Sun, Q. Yue, J. Yang, X. Wang, Y. Deng, C. Yu, D. Zhao, *J. Am. Chem. Soc.* **2014**, *136*, 1884–1892; c) Y. Li, B. P. Bastakoti, M. Imura, S. M. Hwang, Z. Sun, J. H. Kim, S. X. Dou, Y. Yamauchi, *Chem. Eur. J.* **2014**, *20*, 6027–6032; d) Y. Li, W. Luo, N. Qin, J. Dong, J. Wei, W. Li, S. Feng, J. Chen, J. Xu, A. A. Elzatahry, M. H. Es-Saheb, Y. Deng, D. Zhao, *Angew. Chem. Int. Ed.* **2014**, *53*, 9035–9040;

Angew. Chem. **2014**, *126*, 9181 – 9186; e) J. Shim, J. Lee, Y. Ye, J. Hwang, S.-K. Kim, T.-H. Lim, U. Wiesner, J. Lee, *ACS Nano* **2012**, *6*, 6870 – 6881.

[6] a) G. S. Attard, J. M. Corker, C. G. Göltner, S. Henke, R. H. Templer, *Angew. Chem. Int. Ed. Engl.* **1997**, *36*, 1315 – 1317; *Angew. Chem.* **1997**, *109*, 1372 – 1374; b) G. S. Attard, P. N. Bartlett, N. R. Coleman, J. M. Elliott, J. R. Owen, J. H. Wang, *Science* **1997**, *278*, 838 – 840; c) G. S. Attard, S. A. A. Leclerc, S. Maniguet, A. E. Russell, I. Nandhakumar, P. N. Bartlett, *Chem. Mater.* **2001**, *13*, 1444 – 1446; d) C. Li, T. Sato, Y. Yamauchi, *Angew. Chem. Int. Ed.* **2013**, *52*, 8050 – 8053; *Angew. Chem.* **2013**, *125*, 8208 – 8211; e) H. Wang, S. Ishihara, K. Ariga, Y. Yamauchi, *J. Am. Chem. Soc.* **2012**, *134*, 10819 – 10821.

[7] a) L. Wang, Y. Yamauchi, *J. Am. Chem. Soc.* **2013**, *135*, 16762 – 16765; b) G. Surendran, L. Ramos, B. Pansu, E. Prouzet, P. Beaunier, F. Audonnet, H. Remita, *Chem. Mater.* **2007**, *19*, 5045 – 5048; c) P. N. Bartlett, J. J. Baumberg, P. R. Birkin, M. A. Ghanem, M. C. Netti, *Chem. Mater.* **2002**, *14*, 2199 – 2208; d) H. Ataee-Esfahani, M. Imura, Y. Yamauchi, *Angew. Chem. Int. Ed.* **2013**, *52*, 13611 – 13615; *Angew. Chem.* **2013**, *125*, 13856 – 13860.

[8] Y. Yamauchi, A. Sugiyama, R. Morimoto, A. Takai, K. Kuroda, *Angew. Chem. Int. Ed.* **2008**, *47*, 5371 – 5373; *Angew. Chem.* **2008**, *120*, 5451 – 5453.

[9] P. J. Cappillino, K. M. Hattar, B. G. Clark, R. J. Hartnett, V. Stavila, M. A. Hekmaty, B. W. Jacobs, D. B. Robinson, *J. Mater. Chem. A* **2013**, *1*, 602 – 610.

[10] L. Wang, Y. Yamauchi, *Chem. Mater.* **2009**, *21*, 3562 – 3569.

[11] a) J. Chen, T. Herricks, M. Geissler, Y. Xia, *J. Am. Chem. Soc.* **2004**, *126*, 10854 – 10855; b) S. B. Vendelbo, C. F. Elkjær, H. Falsig, I. Puspitasari, P. Dona, L. Mele, B. Morana, B. J. Nelissen, R. van Rijn, J. F. Creemer, P. J. Kooyman, S. Helveg, *Nat. Mater.* **2014**, *13*, 884 – 890.

[12] B. P. Bastakoti, S. Guragain, Y. Yokoyama, S. Yusa, K. Nakashima, *New J. Chem.* **2012**, *36*, 125 – 129.

[13] a) L. Cao, T. Man, M. Kruk, *Chem. Mater.* **2009**, *21*, 1144 – 1153; b) Y. Deng, J. Liu, C. Liu, D. Gu, Z. Sun, J. Wei, J. Zhang, L. Zhang, B. Tu, D. Zhao, *Chem. Mater.* **2008**, *20*, 7281 – 7286; c) M. Kruk, *Acc. Chem. Res.* **2012**, *45*, 1678 – 1687.

[14] J.-F. Gohy, N. Willet, S. Varshney, J.-X. Zhang, R. Jérôme, *Angew. Chem. Int. Ed.* **2001**, *40*, 3214 – 3216; *Angew. Chem.* **2001**, *113*, 3314 – 3316.

[15] a) M. Aizawa, J. M. Buriak, *J. Am. Chem. Soc.* **2006**, *128*, 5877 – 5886; b) L. M. Bronstein, S. N. Sidorov, P. M. Valetsky, J. Hartmann, H. Cölfen, M. Antonietti, *Langmuir* **1999**, *15*, 6256 – 6262; c) S. N. Sidorov, L. M. Bronstein, Y. A. Kabachii, P. M. Valetsky, P. L. Soo, D. Maysinger, A. Eisenberg, *Langmuir* **2004**, *20*, 3543 – 3550.

[16] A. Khanal, Y. Inoue, M. Yada, K. Nakashima, *J. Am. Chem. Soc.* **2007**, *129*, 1534 – 1535.

[17] M. P. Klein, B. W. Jacobs, M. D. Ong, S. J. Fares, D. B. Robinson, V. Stavila, G. J. Wagner, I. Arslan, *J. Am. Chem. Soc.* **2011**, *133*, 9144 – 9147.

[18] H. Wang, L. Wang, T. Sato, Y. Sakamoto, S. Tominaka, K. Miyasaka, N. Miyamoto, Y. Nemoto, O. Terasaki, Y. Yamauchi, *Chem. Mater.* **2012**, *24*, 1591 – 1598.

[19] D. Y. Chung, Y.-H. Chung, N. Jung, K.-H. Choi, Y.-E. Sung, *Phys. Chem. Chem. Phys.* **2013**, *15*, 13658 – 13663.

[20] a) B. Lim, M. Jiang, P. H. C. Camargo, E. C. Cho, J. Tao, X. Lu, Y. Zhu, Y. Xia, *Science* **2009**, *324*, 1302 – 1305; b) M. Yang, Q. Cai, C. Liu, R. Wu, D. Sun, Y. Chen, Y. Tang, T. Lu, *J. Mater. Chem. A* **2014**, *2*, 13738 – 13743.

[21] a) Y. Hu, Q. Shao, P. Wu, H. Zhang, C. Cai, *Electrochem. Commun.* **2012**, *18*, 96 – 99; b) F. Bai, Z. Sun, H. Wu, R. E. Haddad, X. Xiao, H. Fan, *Nano Lett.* **2011**, *11*, 3759 – 3762; c) H. Lv, T. Peng, P. Wu, M. Pan, S. Mu, *J. Mater. Chem.* **2012**, *22*, 9155 – 9160.

Received: June 8, 2015
Revised: July 5, 2015
Published online: August 11, 2015

